Crisis and topological entropy

Yin Shui Fan and Teresa Ree Chay
Department of Biological Sciences, Faculty of Arts and Sciences, University of Pittsburgh, Pittsburgh, Pennsylvania 15260
(Received 22 February 1994)

Topological entropy characterizes the complexity of a dissipative system. Crisis means a sudden collapse in the size of a chaotic attractor or sudden destruction of a chaotic attractor. In this paper, we illustrate that at some interior crises of a dissipative system topological entropy makes a discontinuous change. This intrinsic feature indicates the onset of a crisis in dissipative systems. Using examples of excitable cell models, we estimated topological entropy in terms of the associated Poincaré maps and showed that the topological entropy changes discontinuously when an interior crisis occurs. We also show that at this crisis two opposite bifurcation processes, with very different dynamical complexities, collide with each other in these dissipative systems, and that the collision gives rise to the occurrence of the crisis in a continuous dynamical system.

PACS number(s): 05.45.+b

Sudden qualitative changes in chaotic dynamical behavior have been observed in dissipative systems, such as those that occur in plasmas, fluids, stochastic resonance, and excitable cell systems [1]. Such sudden changes have been termed *crises* [2], and include *boundary crisis* and *interior crisis*. At the crisis, certain characteristic statistical behavior of a dissipative system occurs. For example, the number of unstable periodic orbits embedded within a chaotic attractor suddenly increases or decreases at the crisis [3,4]. Accordingly, the complexity of a dissipative system will change at the crisis. Traditionally, the Lyapunov exponent and the topological entropy are used to indicate the complexity of dissipative systems. In this paper, we show that for some crisis phenomena the Lyapunov exponent no longer provides convincing evidence, and we illustrate that the topological entropy for a chaotic system makes a discontinuous change at the crisis. This intrinsic feature may provide evidence for the crisis. Using examples of excitable cell models in the Appendix (which include the Rose-Hindmarsh model for neuron cell activity and the Chay model for pancreatic β-cell activity), we estimate the topological entropy in terms of the associated Poincaré maps of these systems. It turns out that the topological entropy for these systems makes a discontinuous change at the crisis. That is, as a system parameter passes through a threshold value, the complexity of the systems suddenly increases or decreases. Such a sudden change in the complexity of a dissipative system (or discontinuous change in its topological entropy) indicates the occurrence of the crisis in these continuous dynamical systems.

CRISIS TRANSITION BETWEEN DIFFERENT CHAOS

The bifurcation diagrams in Figs. 1(a) and 1(b) are obtained by numerically integrating Eq. (A1), in the Appen-

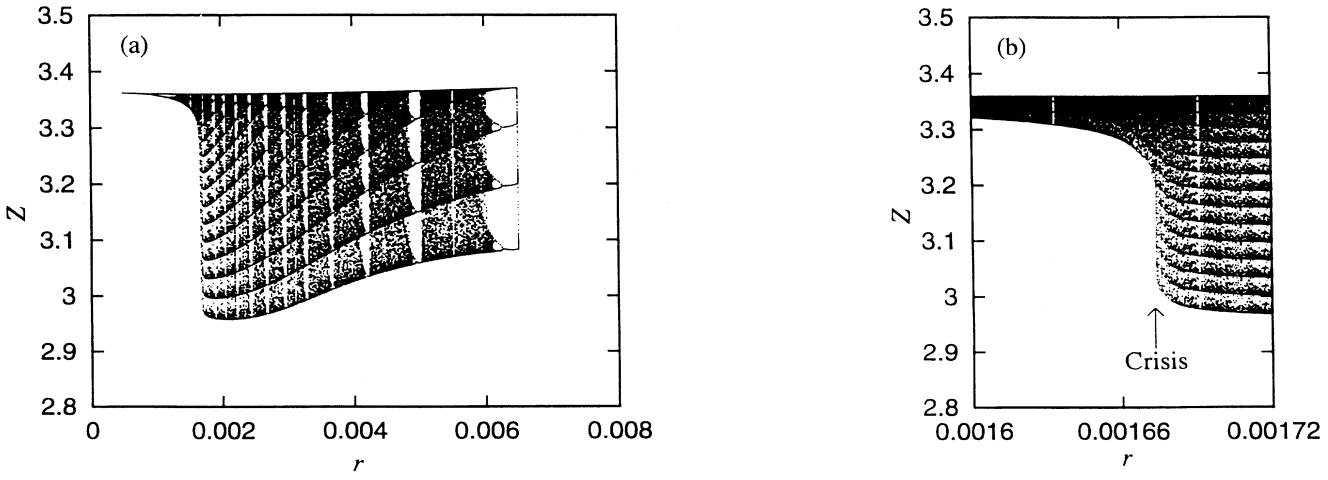

FIG. 1. Bifurcation diagrams obtained by integrating Eq. (A1), (a) for $I=3.281$ with r as the bifurcation parameter, and (b) the enlargement of the part of (a) over the interval of $r\in[0.0016, 0.001\,72]$ indicated by a bar in (a). They both show that a crisis occurs at $r_c=0.001\,673$ and two opposite bifurcation processes collide with each other at the crisis.

dix. The diagrams show that an apparent sudden collapse in the size of a chaotic attractor occurs at a value of the parameter $r=0.001\,673$ (denoting the crisis value by r_c). Such a sudden qualitative change in a chaotic attractor is known as *interior crisis* [2]. To compare the structures of chaotic attractors in the right and left of the crisis point, we illustrate a chaotic attractor for $r=0.001\,672$ ($<r_c$, slightly) in Fig. 2(a), and a chaotic attractor for $r=0.001\,674$ ($>r_c$, slightly) in Fig. 2(b), respectively. The structure of the chaotic attractor in Fig. 2(a) is very similar to that of the top part of the attractor in Fig. 2(b), but it is qualitatively different from the structure of the whole attractor in Fig. 2(b). At the crisis, the chaotic attractor dramatically extends or shrinks in size. That is, at the crisis, the qualitative structure of the chaotic attractor is suddenly changed. The attractor shown in Fig. 2(a) corresponds to chaotic spiking (only fast irregular oscillations); the chaotic attractor shown in Fig. 2(b) corresponds to chaotic bursting (between spikes there are some slow periods or plateaus of action potential x). This crisis, occurring at r_c, bridges two different types of chaos, chaotic spiking and chaotic bursting.

For $r>r_c$, numerical computation gives the (saddle-node) bifurcation values: $r_3=0.010\,25$, $r_4=0.006\,49$, $r_5=0.005\,02$, $r_6=0.004\,24$, $r_7=0.003\,71$, $r_8=0.003\,31$, $r_9=0.002\,98$, $r_{10}=0.0027$, $r_{11}=0.002\,46$, $r_{12}=0.002\,25$, $r_{13}=0.002\,065$, $r_{14}=0.001\,895$, $r_{15}=0.001\,727$, at which the system of Eq. (A1) yields superstable period 3, 4,..., 15, respectively. So, before the crisis ($r>r_c$) and as the parameter r is decreased the system evolves in the following way:

period 3 → period-doubling cascades and chaos → saddle-node bifurcation →

period 4 → period-doubling cascades and chaos → saddle-node bifurcation →

period 5 → period-doubling cascades and chaos → saddle-node bifurcation →

...

period 15 → period-doubling cascades and chaos →

crisis.

We note in Fig. 1(a) that the right part of the bifurcation diagram, where the period-3 window exhibits, is omitted. During the above process, the period of superstable periodic orbit is increased as r is decreased.

For $r<r_c$, the system undertakes saddle-node bifurcations at $r_3^*=0.001\,52$ and $r_4^*=0.001\,632\,5$, at which the system generates superstable period 3 and period 4, respectively. So, after the crisis ($r<r_c$) and as the parameter r is decreased further, the system evolves in an inverse bifurcation process:

crisis → chaos and inverse period-doubling bifurcation [5,6] →

...

period 3 → inverse saddle-node bifurcation → chaos and inverse period-doubling bifurcation →

period 2 →

period 1.

During the inverse bifurcation process, the period of the superstable periodic orbits is decreased as the parameter r decreases. Evidently, two opposite bifurcation processes collide with each other at the crisis point ($r=r_c$). We will subsequently see that the complexities of the dynamical system are quite different before and after the crisis. In this situation, it is impossible for the physical dissipative system to evolve smoothly from one chaotic regime to another completely different chaotic regime. For example, the system of Eq. (A1) does not evolve smoothly from chaotic bursting to chaotic spiking. Thus, a crisis occurs between these two chaotic regimes, chaotic spik-

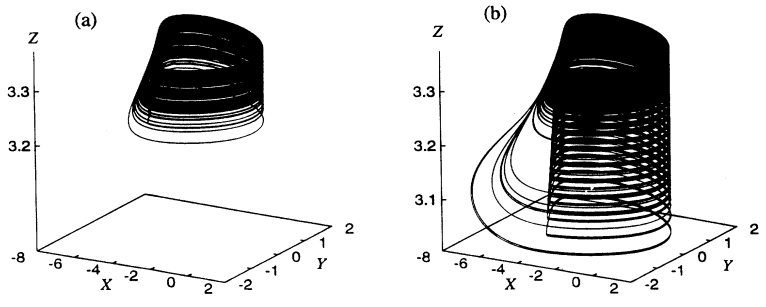

FIG. 2. Chaotic attractors obtained by integrating Eq. (A1), (a) for $I=3.281$ and $r=0.001\,672$, slightly left of the crisis point; (b) for $I=3.281$ and $r=0.001\,674$, slightly right of the crisis point.

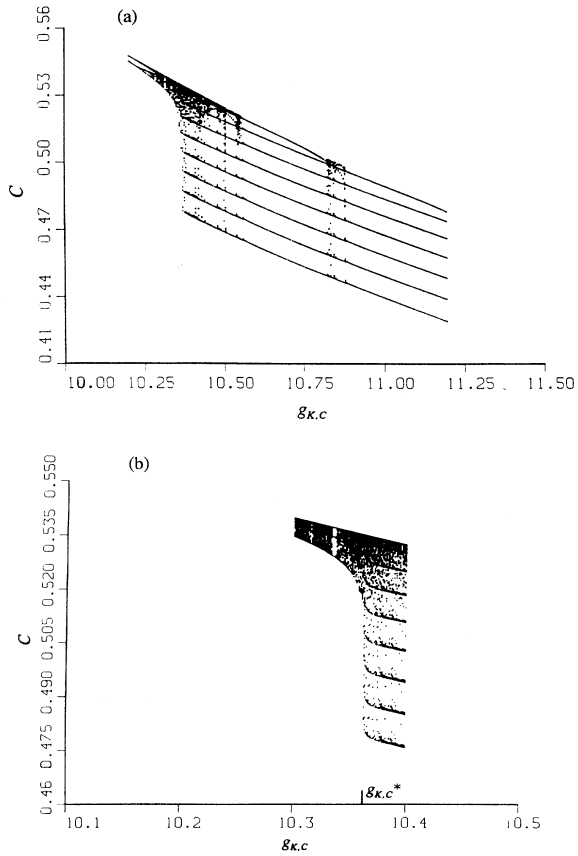

FIG. 3. Bifurcation diagrams obtained by integrating Eq. (A2), (a) for $\lambda_n = 236$ with $g_{K,C}$ as the bifurcation parameter; and (b), the enlargement of the part of (a) over the interval $g_{K,C} \in [10.3, 10.4]$, show a crisis occurs at $g_{K,C}^* = 10.3625$ and two opposite bifurcation processes collide with each other at the crisis.

ing and chaotic bursting, at the threshold value r_c. This is an example of a crisis transition between two different chaotic regimes in a physical dissipative system.

Such a crisis phenomenon is also observed in pancreatic β-cell model, Eq. (A2) in the Appendix. The bifurcation diagrams in Figs. 3(a) and 3(b) show that a crisis occurs at a value $g_{K,C}^* = 10.3625$. Similar to that in the system of Eq. (A1), this crisis makes a transition between two different chaotic regimes, and is formed by a collision between opposite bifurcation processes with quite different complexities at the threshold value of $g_{K,C} = 10.3625$.

LYAPUNOV EXPONENT MAY NOT BE EVIDENCE FOR SUCH A CRISIS

Traditionally, the Lyapunov exponent is used to indicate the complexity of a chaotic dynamical system. Preferably, it is used to distinguish a periodic behavior from chaos. Nevertheless, the Lyapunov exponent is hard to distinguish two different types of chaos, such as chaotic bursting and chaotic spiking. In particular, the Lyapunov exponent will not provide convincing evidence for the crisis transition between two different types of chaos. To support this point, we present the Lyapunov exponent spectra in Fig. 4(a) for Eq. (A1), with the same parameters as in Fig. 1(a). It gives clear diagnoses for bifurcations and chaos, but not for the crisis at $r = r_c$. Over the intervals on which the system exhibits chaos, the Lyapunov exponent spectra takes a form $(\lambda_1, \lambda_2, \lambda_3) = (+, 0, -)$; over the intervals in which the system exist stable periodic orbits, the Lyapunov exponent spectra takes a form $(\lambda_1, \lambda_2, \lambda_3) = (0, -, -)$; at each saddle-node bifurcation, the largest Lyapunov exponent λ_1 changes from positive to zero, and the second largest exponent λ_2 changes from zero to negative; at each period-doubling bifurcation, λ_2 approaches the line of $\lambda = 0$. However, the Lyapunov exponent spectra does not provide any signs for the crisis at $r = r_c$, as shown in Figs. 4(a) and 4(b) (an enlargement of 4(a) over the interval of $r \in [0.0016, 0.0017]$ which is marked in 4(a)). This failure shows that the Lyapunov exponent is not able to distinguish different chaotic regimes and does not provide convincing evidence for the crisis between the two different types of chaos. To provide convincible evidence of such interior crisis, we will now estimate topological entropy in terms of the associated Poincaré maps of the dissipative system.

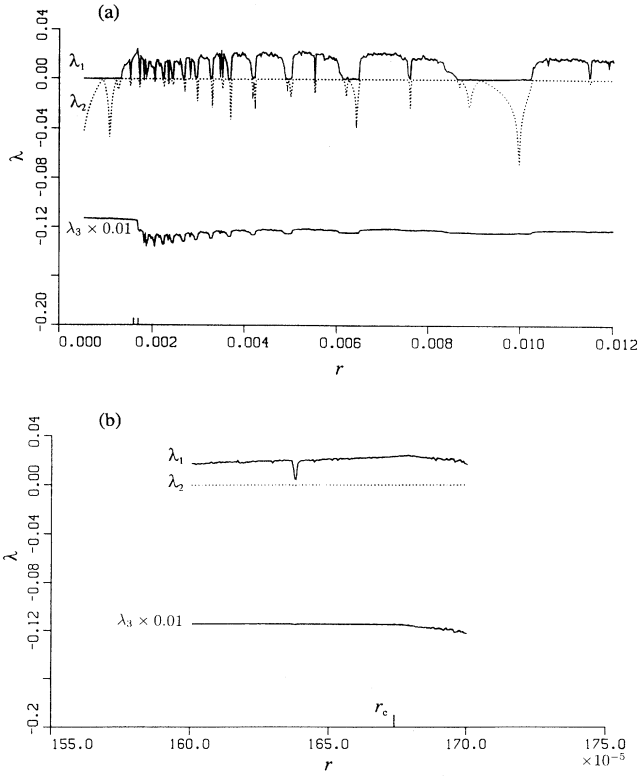

FIG. 4. Lyapunov exponent spectra $\lambda_1 > \lambda_2 > \lambda_3$ versus the bifurcation parameter r for Eq. (A1), (a) for the same value of I as in Fig. 1(a); (b) an enlargement of the part of (a) over the interval of $r \in [0.0016, 0.0017]$ which is marked in (a).

ESTIMATING TOPOLOGICAL ENTROPY FROM THE POINCARÉ MAPS

Topological entropy is another characteristic exponent that indicates the complexity of a dissipative system. A possible way of defining the topological entropy $H(f)$ of a map f is given by [7,8]

$$H(f)=\lim_{m\to\infty}\ln N(f^m)/m \ , \tag{1}$$

where $N(f^m)$ denotes the number of fixed points of the mth iteration of f. To compute topological entropy, we numerate the number $N(f^m)$ of the period-m orbits for an associated Poincaré map f (or the number of fixed points of the mth iteration of the map f).

Case 1. For any integer $n\geq 3$, let f be the Poincaré map and possess a superstable period-n orbit. Namely, the kneading sequence [9] of the Poincaré map f takes the following form:

$$cR(L)^{n-2} \ . \tag{2}$$

Here, c denotes the critical point of the Poincaré map f. The n superstable periodic points give the following Markov partition [10] on the interval $\Lambda=[f^2(c),f(c)]$:

$$\alpha_1=[f^2(c),f^3(c)], \quad \alpha_2=[f^3(c),f^4(c)], \ldots ,$$

$$\alpha_{n-2}=[f^{n-1}(c),c], \ \alpha_{n-1}=[c,f(c)] \ ,$$

where $f^n(c)=c$, The orbit starting from any initial point will approach and stay on the interval, $\Lambda=\alpha_1\cup\alpha_2\cup\cdots\cup\alpha_{n-1}$. [For example, Fig. 5(a) shows a Poincaré map with a superstable period-6 orbit and a kneading sequence $cR(L)^4$.] In this case, the Poincaré map f acts on these intervals, $\alpha_1, \alpha_2, \ldots, \alpha_{n-1}$, in the following fashion:

$$\begin{aligned} f:\ & \alpha_1\to\alpha_2 \\ & \alpha_2\to\alpha_3 \\ & \cdots \\ & \alpha_{n-2}\to\alpha_{n-1} \\ & \alpha_{n-1}\to\alpha_1+\alpha_2+\cdots+\alpha_{n-2}+\alpha_{n-1} \ . \end{aligned}$$

This transformation can be represented by a transition matrix [10]

$$A=\begin{bmatrix} 0 & 1 & 0 & \cdots & 0 & 0 \\ 0 & 0 & 1 & \cdots & 0 & 0 \\ 0 & 0 & 0 & \cdots & 1 & 0 \\ \cdots & \cdots & \cdots & \cdots & \cdots & \cdots \\ 0 & 0 & 0 & .... & 0 & 1 \\ 1 & 1 & 1 & \cdots & 1 & 1 \end{bmatrix}_{(n-1)\times(n-1)} . \tag{3}$$

The transition matrix $A=[A_i]$ is constructed with $A_i=1$ if $f(\alpha_i)\supset\alpha_j$, and zero otherwise. The characteristic equation of matrix A is given as follows:

$$\lambda^{n-1}-\lambda^{n-2}-\cdots-\lambda-1=0 \ . \tag{4}$$

The number of the period-m orbits of the map f is governed by the following recursive relation (for more detail, see Ref. [11]):

$$N(f^m)=N(f^{m-1})+N(f^{m-2})+\cdots+N(f^{m-(n-1)}) \ ,$$
$$m=n,n+1,\ldots . \tag{5}$$

Particularly, for $n=3$, recursive relation (5) gives the Fibonacci numbers. Let $\lambda_1,\lambda_2,\ldots,\lambda_{n-1}$ be the roots of Eq. (4) and denote $\lambda_{\max}=\max\{\lambda_1,\lambda_2,\ldots,\lambda_{n-1}\}$. Then the number $N(f^m)$ of the period-m orbits of f meets the following relation [11]:

$$N(f^m)=\mathrm{Tr}[A^m]=\lambda_1^m+\lambda_2^m+\cdots+\lambda_{n-1}^m \ ,$$
$$m=1,2,\ldots . \tag{6}$$

The topological entropy $H(f)$ is given by

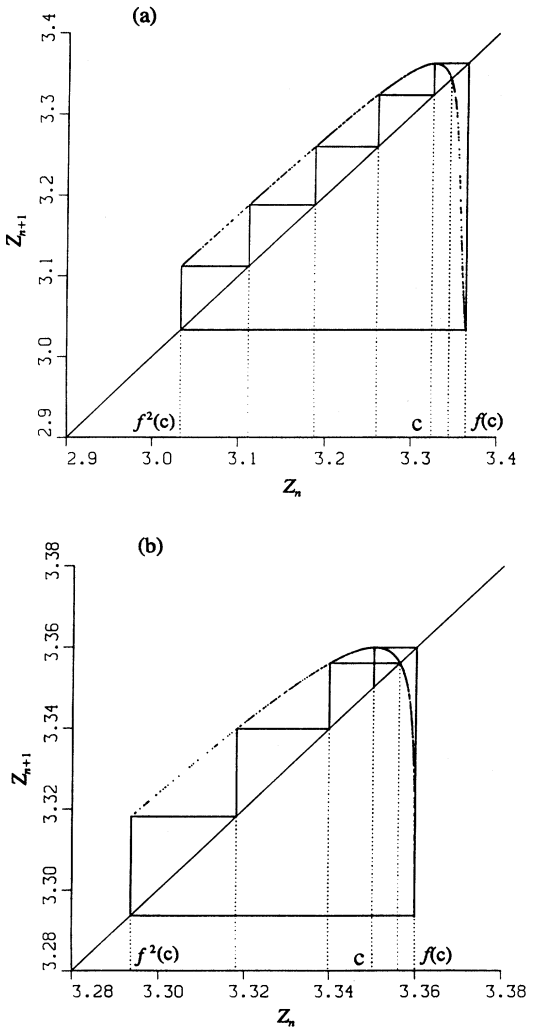

FIG. 5. Poincaré maps obtained by integrating Eq. (A1). (a) for $I=3.281$ and $r=0.004\,25$, showing a Poincaré map with superstable period-6 orbit and the kneading sequence $cR(L)^4$; (b) $I=3.281$ and $r=0.001\,65$, showing a Poincaré map with a kneading sequence $cR(L)^3R$.

$$H(f)=\lim_{m\to\infty}\ln N(f^m)/m$$
$$=\lim_{m\to\infty}\ln(\lambda_1^m+\lambda_2^m+\cdots+\lambda_{n-1}^m)/m$$
$$=\ln\lambda_{\max}\ . \tag{7}$$

Case 2. Let g be a Poincaré map and have the following kneading sequence:

$$cR(L)^{n-2}R\ . \tag{8}$$

[For example, Fig. 5(b) shows a Poincaré map that possesses a kneading sequence $cR(L)^3R$.] In this case, the corresponding transition matrix B takes the following form:

$$B=\begin{bmatrix} 0 & 1 & 1 & 0 & \cdots & 0 & 0 \\ 0 & 0 & 0 & 1 & \cdots & 0 & 0 \\ \cdots & \cdots & \cdots & \cdots & \cdots & \cdots & \cdots \\ 0 & 0 & 0 & 0 & \cdots & 0 & 1 \\ 0 & 0 & 0 & 0 & \cdots & 0 & 1 \\ 1 & 1 & 1 & 1 & \cdots & 1 & 0 \end{bmatrix}_{n\times n},$$

and with the characteristic equation

$$\eta^n-2\eta^{n-2}-\cdots-2\eta^2-2\eta=0\ . \tag{9}$$

The number of fixed points of the mth iteration of the Poincaré map g is governed by the following recursive relation:

$$N(g^m)=2N(g^{m-2})+2N(g^{m-3})+\cdots+2N(g^{m-(n-1)})\ ,$$
$$m=n,n+1,\ldots\ . \tag{10}$$

Let $\eta_1,\eta_2,\ldots,\eta_n$, be the roots of Eq. (10), and $\eta_{\max}=\max\{\eta_1,\eta_2,\ldots,\eta_n\}$; then, $N(g^m)=\eta_1^m+\eta_2^m+\cdots+\eta_n^m$. Thus, the topological entropy $H(g)$ is given by

$$H(g)=\lim_{m\to\infty}\ln N(g^m)/m$$
$$=\lim_{m\to\infty}\ln(\eta_1^m+\eta_2^m+\cdots+\eta_n^m)/m$$
$$=\ln\eta_{\max}\ . \tag{11}$$

We note here that, in the bifurcation process schematized in Fig. 1(a), the value of the parameter r responsible for the presence of the kneading sequence $cR(L)^{n-2}R$ is located between the values of r responsible for the kneading sequences, $cR(L)^{n-1}$ and $cR(L)^n$.

TOPOLOGICAL ENTROPY AS A DIAGNOSIS FOR CRISIS

From formulas (7) and (11), we can estimate the topological entropy for certain values at which the associated Poincaré maps have the kneading sequence (2) or (8).

For $r>r_c$, the system undergoes saddle-node bifurcations at $r_3,r_4,\ldots,r_{15}$; for $r<r_c$, the system undergoes (inverse) saddle-node bifurcation at $r_4^*=0.001\,632\,5$ and

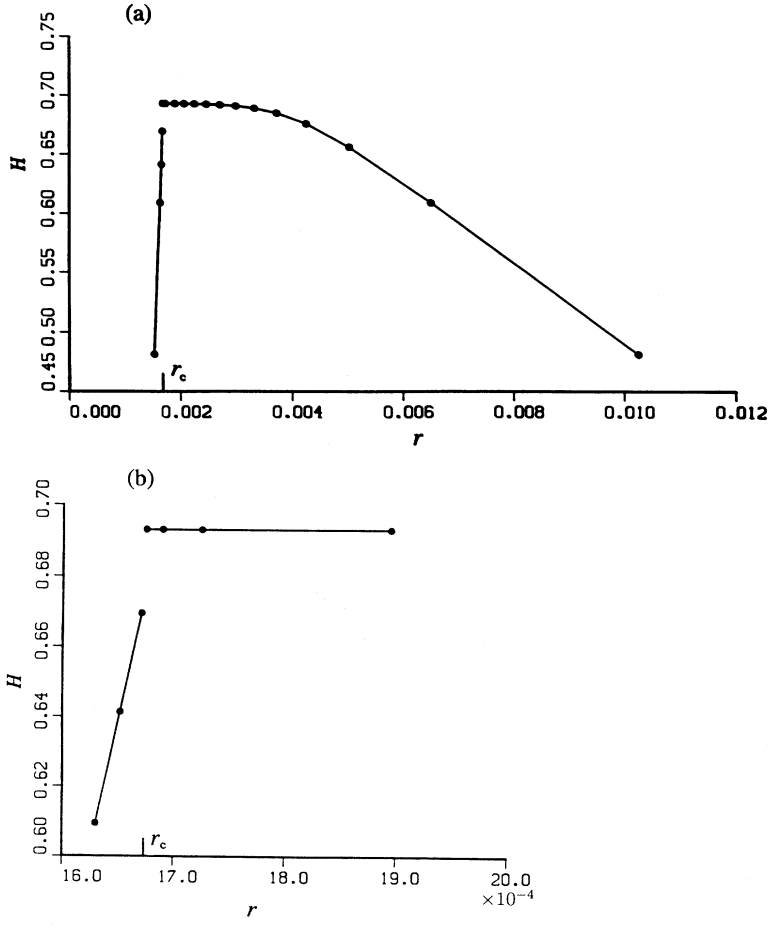

FIG. 6. Topological entropy H versus r for Eq. (A1), (a) for the same value of I as in Figs. 1(a) and 4(a); (b) an enlargement of the part of (a) over the interval of $r\in[0.001\,63,0.0019]$, shows a sudden discontinuity in topological entropy at $r_c=0.001\,673$.

$r_3^* = 0.001\,52$, at which the system generates superstable period-4 and superstable period-3 orbits.

At each saddle-node bifurcation point, topological entropy H can be computed from Eq. (7). At $r = 0.001\,652$, $r = 0.001\,67$ ($< r_c$, slightly), and $r = 0.001\,676$ ($> r_c$, slightly), the corresponding Poincaré maps have the kneading sequences

$$cR(L)^2R, \quad cR(L)^5R, \quad cR(L)^{14}R ,$$

which take the form of Eq. (8). So, the topological entropy at $r = 0.001\,652$, 0.001 67, and 0.001 676 can be calculated from Eq. (11).

Figure 6(a) shows the topological entropy H versus the bifurcation parameter r for Eq. (A1); Fig. 6(b) is an enlargement of Fig. 6(a) over the interval of $r \in [0.001\,63, 0.0019]$. These plots illustrate that the topological entropy H versus r has a discontinuity at the crisis point ($r = r_c$). It implies that the complexity of the dissipative system suddenly changes at the crisis. Before the crisis ($r > r_c$) and as r decreases, the topological entropy H monotonically increases, which is associated with the increase in the period of superstable orbits; after the crisis ($r < r_c$) and as r decreases, the topological entropy H monotonically decreases. Both the bifurcation diagrams in Fig. 1 and topological entropies in Fig. 6 show that, before and after the crisis, the dissipative system evolves in opposite bifurcation processes, and the two opposite processes collide with each other. The collision of two opposite bifurcation processes with quite different complexities then causes the crisis.

A collision of two opposite bifurcation processes with different system complexities leading to a crisis can also be seen in Eq. (A2). Figure 3(a) is the bifurcation diagram for Eq. (A2). Figure 7, obtained for Eq. (A2), shows topological entropy versus the bifurcation parameter $g_{K,C}$. Both Fig. 3 and Fig. 7 show that a crisis occurs at a value of $g_{K,C} = 10.3625$. On the right and left of the crisis, there exist two opposite bifurcation processes. Figure 7 shows that a discontinuity in the topological entropy occurs at the crisis, and that as these two bifurcation processes collide the system takes on quite different dynamical complexities. This gives another example of how two opposite bifurcation processes with different dynamical complexities (different topological entropies) can collide to bring about a crisis in a dissipative system.

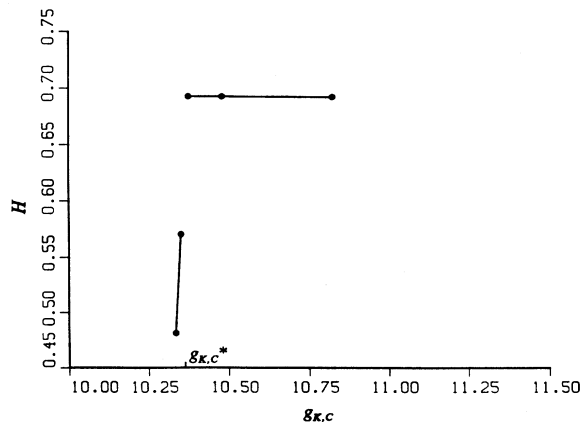

FIG. 7. Topological entropy H versus $g_{K,C}$ for Eq. (A2), with the same value of λ_n as in Figs. 3(a) and 3(b), shows a sudden discontinuity in dynamical complexity at $g_{K,C}^* = 10.3625$.

A SCALING RATIO SEQUENCE FOR A PERIOD-ADDING SEQUENCE

To account for the above crisis mechanism, we consider a scaling sequence for a period-adding sequence that appears in the evolution of dissipative systems. For example in Fig. 1(a), for $r > r_c$, there undergoes a series of saddle-node bifurcations at $r_3, r_4, \ldots, r_{15}$. These saddle-node bifurcations are associated with a period-adding sequence, superstable period 3,4, . . . , 15.

Generally, we suppose that such a period-adding sequence will extend infinitely in a dissipative system, and, the sequence of saddle-node bifurcation values is given by

$$\{\gamma_i\}_{i=3}^{\infty} . \tag{12}$$

Consider the ratios,

$$\delta_i = (\gamma_{i+2} - \gamma_{i+1})/(\gamma_{i+1} - \gamma_i) , \quad i = 3,4,\ldots . \tag{13}$$

We call sequence (13) the *scaling sequence* of the period-adding sequence, and call $\lim_{i\to\infty}\delta_i$ the *scaling number* of the period-adding sequence. Elsewhere [12] we have obtained a period-adding scaling sequence

$$\{\delta_i = (i-2)/i\}_{i=3}^{\infty} \tag{14}$$

with a scaling number,

$$\delta = \lim_{i\to\infty}\delta_i = 1 . \tag{15}$$

We conjectured that, like the Feigenbaum scaling number, the scaling ratio sequence (14) and the scaling number (15) of the period-adding sequence are universal in dissipative system evolutions [13].

For example, the sequence $\{r_i\}_{i=3}^{15}$ gives the first 11 terms of the scaling ratio sequence associated with the saddle-node bifurcations schematized in Fig. 1(a):

$$\begin{aligned} &\delta_3 = 0.390\,957, \quad \delta_4 = 0.5306, \quad \delta_5 = 0.6795 , \\ &\delta_6 = 0.7547, \quad \delta_7 = 0.825, \quad \delta_8 = 0.8485 , \\ &\delta_9 = 0.8571, \quad \delta_{10} = 0.875, \quad \delta_{11} = 0.881 , \\ &\delta_{12} = 0.919, \quad \delta_{13} = 0.9294 , \end{aligned} \tag{16}$$

and, from δ_5 on, the terms of the sequence (16) almost coincide with the corresponding terms of sequence (14).

One can imagine that, in Fig. 1(a) and for r slightly less than r_c, if the system possesses the same topological entropy (the same dynamical complexity) as that of before the crisis ($r < r_c$, slightly), the system will smoothly evolve from one bifurcation process to the opposite bifurcation process. That is, if for r slightly less than r_c the system generates a superstable period-15 orbit, the dynamical complexity will match with that for r slightly greater than r_c, and the system may get rid of the crisis at r_c. To support this point, we present a bifurcation dia-

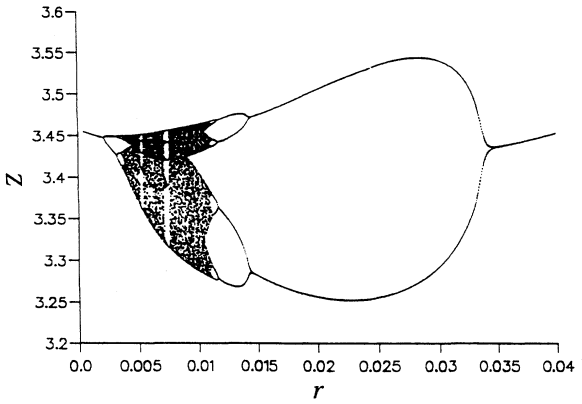

FIG. 8. Bifurcation diagram, obtained by integrating Eq. (A1) for $I=3.375$, shows that the system of Eq. (A1) can smoothly evolve from one bifurcation process to the opposite bifurcation process.

gram shown in Fig. 8 by integrating Eq. (A1) for $I=3.375$. This diagram gives an example of how the system can smoothly transfer from one bifurcation process to the opposite bifurcation process. Over the interval of $r\in[0.0054, 0.0073]$, the two opposite bifurcation processes collide with each other, but no crisis occurs. The reason for this is that the dynamical complexities (or topological entropies) on the right and the left bifurcation process are matchable. As seen in Fig. 8, both the right and left bifurcation processes generate superstable period-5 orbits as they collide with each other over the interval of $r\in[0.0054,0.0073]$.

Since the scaling sequence (16) associated with the (right) period-adding process in Fig. 1(a) is universal, the left ($r<r_c$) bifurcation process in Fig. 1(a) should evolve at the same rate as described by the scaling sequence. Suppose the left bifurcation process in Fig. 1(a) can keep evolving at the same rate. In this process, for what value of the parameter r the system will undergo a saddle-node bifurcation that generates the superstable period 15? In other words, for what value of r the topological entropy in the left bifurcation process will match with that in the right bifurcation process near the crisis? Using the scaling sequence (16), we can obtain an approximate value r^* at which the left bifurcation process will undergo a saddle-node bifurcation and generate superstable period 15. The value of r^* is estimated as follows:

$$r^*=r_4^*+r_{3,4}^*\{\delta_3+\delta_3\delta_4+\cdots+\delta_3\delta_4\cdots\delta_{13}\}$$
$$=0.001\,773\,73\ ,$$

where $r_{3,4}^*=r_4^*-r_3^*$. However, this value is much greater than the real crisis value $r=r_c$. This implies that a premature collision of two opposite bifurcation processes occurs, and that the complexities of the two opposite bifurcation processes are not matchable. This collision then brings about the crisis at $r=r_c$.

In conclusion we have shown that the topological entropy H of a dissipative system has an apparent discontinuity at some interior crises, and that the occurrence of such an interior crisis is due to the collision of two opposite bifurcation processes with quite different complexities. The discontinuity in the topological entropy of the associated Poincaré map means a sudden change of the dynamical complexity in dissipative systems. The topological entropy is one of key characteristic statistical behavior in a dissipative system. We therefore believe that the discontinuous change in the topological entropy is sufficient for such an interior crisis and indicates the occurrence of the crisis in a physical dissipative system.

ACKNOWLEDGMENTS

This work was supported by the Pennsylvania Affiliate of the American Heart Association Foundation and by NSF DCB-8819245. This research was also supported in part by the Pittsburgh Supercomputer Center through Agreement U41 RR0415.

APPENDIX

The Rose-Hindmarsh model is three differential equations [14]:

$$\begin{aligned} dx/dt&=y-ax^3+bx^2+I-z\ ,\\ dy/dt&=c-dx^2-y\ ,\\ dz/dt&=r[S(x-x_1)-z]\ , \end{aligned}\tag{A1}$$

where t is time, x represents membrane potential, y is a recovery variable, and z is the adaptation current. I, applied current, and r are control parameters. In the above equation, a, b, c, d, S, and x_1 are constants. We here use the values $a=1.0$, $b=3.0$, $c=1.0$, $d=5.0$, $S=4.0$, and $x_1=-1.6$.

The Chay model consists of three differential equations [15]:

$$\begin{aligned} dV/dt&=1800m_\infty^3h_\infty(100-V)+1700n^4(75-V)\\ &\quad+g_{K,C}C/(1+C)(-40-V)+7(100-V)\ ,\\ dC/dt&=27\{m_\infty^3h_\infty(V_C-V)-0.1833C\}/100\ ,\\ dn/dt&=(n_\infty-n)/\tau_n\ , \end{aligned}\tag{A2}$$

where V is the membrane potential, C the dimensionless calcium concentration, and n a probability of activation. Let y stand for h, m, or n, then the explicit expressions for h_∞, m_∞, and n_∞ can be written as

$$y_\infty=\alpha_y/(\alpha_y+\beta_y)$$

with

$$\begin{aligned} \alpha_h&=0.07\exp(-0.05V-2.5)\ ,\\ \beta_h&=1/[1+\exp(-0.1V-2)]\ ,\\ \alpha_m&=0.1(25+V)/[1-\exp(-0.1V-2.5)]\ ,\\ \beta_m&=4\exp[-(V+50)/18]\ ,\\ \alpha_n&=0.01(20+V)/[1-\exp(-0.1V-2)]\ ,\\ \beta_n&=0.125\exp[-(V+30)/80]\ , \end{aligned}$$

and

$$\tau_n=1/[\lambda_n(\alpha_n+\beta_n)]\ ,$$

$g_{K,C}$ and λ_n are the system parameters.

[1] H. L. Swinney and J. P. Gollub, Phys. Today **31** (8), 41 (1978); J. M. Wersinger, J. M. Finn, and E. Ott, Phys. Rev. Lett. **44**, 453 (1980); G. Ahlers and R. W. Walden, *ibid.* **44**, 445 (1980); M. Giglio, S. Musazzi, and U. Perini, *ibid.* **47**, 243 (1981); W. Lauterborn and E. Cramer, *ibid.* **47**, 1445 (1981); J. Testa, J. Perez, and C. Jeffries, *ibid.* **48**, 714 (1982); K. Ikeda and D. Akimoto, *ibid.* **48**, 617 (1982); T. L. Carroll and L. M. Pecora, *ibid.* **70**, 576 (1993); A. V. Holden and Y. S. Fan, Chaos Solitons Fractals **2**, 583 (1992).

[2] C. Grebogi, E. Ott, and J. A. Yorke, Phys. Rev. Lett. **48**, 1507 (1982); Physica D **7**, 181 (1983).

[3] Y. C. Lai, C. Grebogi, and J. A. Yorke, *Applied Chaos,* edited by J. H. Kim and J. Stringer (Wiley, New York, 1992), p. 441.

[4] Y. S. Fan and T. R. Chay, Chaos Solitons Fractals **3**, 603 (1993).

[5] A. V. Holden and Y. S. Fan, Chaos Solitons Fractals, **2**, 221 (1992).

[6] S. P. Dawson, C. Grebogi, and H. Koçak, Phys. Rev. E **48**, 1676 (1993); L. Stone, Nature (London) **365**, 617 (1993). (In these articles, the authors called the inverse period-doubling bifurcations the reversals of period-doubling bifurcations.)

[7] J. P. Crutchfield and N. H. Packard, Physica D **7**, 201 (1983).

[8] B. L. Hao, Physica D **51**, 161 (1991).

[9] J. Milnor and W. Thurston, in *Dynamical Systems, Proceedings of the Special Year held at the University of Maryland, College Park, 1986–87,* edited by James C. Alexander, Lecture Notes in Mathematics Vol. 1342 (Springer, Berlin, 1988), p. 465.

[10] J. Guchenheimer and P. Holmes, *Nonlinear Oscillations, Dynamical Systems, and Bifurcations of Vector Fields* (Springer-Verlag, Berlin, 1983).

[11] Y. S. Fan and T. R. Chay, Physica D (to be published).

[12] A. V. Holden and Y. S. Fan, Chaos Solitons Fractals **2**, 349 (1992) [In the paper, the authors have constructed a class of maps which undergo period-adding bifurcations and have obtained the sequence of period-adding bifurcation values. From this sequence of bifurcation values, one can see that the scaling ratio for period-adding bifurcation sequence satisfies $\delta=\lim_{i\to\infty}\delta_i=1$, see pp. 363–365.]

[13] Y. S. Fan and T. R. Chay (unpublished).

[14] J. L. Hindmarsh and R. M. Rose, Nature (London) **296**, 162 (1982); Proc. R. Soc. London Ser. B **221**, 87 (1984).

[15] T. R. Chay, Physica D **16**, 233 (1985).